Twenty-Sixth Symposium (International) on Combustion/The Combustion Institute, 1996/pp. 2199–2205

OXYGEN ATOM CONCENTRATIONS AND NO PRODUCTION RATES IN A TURBULENT H_2/N_2 JET FLAME

R. S. BARLOW AND G. J. FIECHTNER
Combustion Research Facility
Sandia National Laboratories
Livermore, CA 94551-0969, USA

J.-Y. CHEN
Department of Mechanical Engineering
University of California
Berkeley, CA 94720, USA

An experimental procedure is demonstrated that allows determination of instantaneous oxygen-atom concentrations and thermal NO production rates in turbulent flames. This is accomplished without direct measurement of O atoms by laser-induced fluorescence, a technique that has been shown to be problematic. Simultaneous point measurements of temperature, the major species, OH, and NO are performed in a non-premixed turbulent jet flame of nitrogen-diluted hydrogen fuel. The O-atom concentration for each laser shot is derived from these data, based on the assumption of partial equilibrium of the reaction OH + OH = O + H_2O. The derived O-atom concentration is then used with the measured N_2 concentration and temperature to calculate the instantaneous thermal (Zeldovich) NO production rate. The partial equilibrium assumption is shown to be appropriate in this flame for conditions relevant to thermal NO formation. The maximum conditionally averaged O-atom mole fraction is about 6.5 times the maximum value for full chemical equilibrium. The width in mixture fraction coordinates of the conditionally averaged NO production rate curve is roughly twice that calculated from adiabatic equilibrium values of temperature, [O], and N_2. Experimental results are compared with predictions obtained using the Monte Carlo PDF model with detailed chemistry. With some exceptions, there is good agreement between experiment and prediction when results are plotted against mixture-fraction (scatter plots and conditional averages). Agreement is not as good when radial profiles of averaged scalar quantities are compared. This indicates that the present PDF model predicts the hydrogen and nitrogen chemistry with good accuracy but that improvements are needed in the modeling of the turbulent fluid dynamics and mixing. A comparison of experimental results with steady strained laminar flame calculations shows that the turbulent flame conditions cannot be represented by a combination of the laminar flames.

Introduction

Thermal NO formation is a significant mechanism in many combustion applications. Considerable research has been carried out using gas-sampling probes to determine the effects of various parameters on NO_x formation in turbulent jet flames [1–6]. More recently, simultaneous laser-based measurements of multiple species have been used to investigate NO formation in hydrogen jet flames [7–10], in laminar CH_4-air Bunsen flames [11], and in bluff-body-stabilized flames [12]. In much of this work, there has been speculation regarding the effects of turbulence-chemistry interactions on superequilibrium levels of O atoms, which contribute to NO production. Experimental O-atom concentrations and thermal NO production rates would be useful in developing a better understanding of the influence of turbulence-chemistry interactions on NO formation and in evaluating various modeling approaches. Investigations of laser-induced fluorescence (LIF) detection of O atoms in laminar flames [13,14] suggest that quantitative single-shot measurements of O-atom concentrations in turbulent flames would be a difficult challenge because the 226-nm laser that excites the O atoms produces additional O atoms by photolysis.

In the present study, we demonstrate an experimental alternative to direct LIF measurements of O-atom concentrations. Pulsed-laser diagnostics are used to obtain simultaneous point measurements of temperature, the major species, OH, and NO. The instantaneous O-atom concentration is derived from the measured temperature, [OH], and [H_2O], based on the assumption of partial equilibrium of the reaction:

$$OH + OH \Leftrightarrow O + H_2O \quad (R1)$$

such that

$$[O] = K_{EQ,1}\,[OH]^2/[H_2O] \quad (1)$$

The thermal NO production rate is then calculated on a shot-to-shot basis from the extended Zeldovich mechanism:

$$N_2 + O \rightarrow N + NO \quad (R2)$$

$$N + O_2 \rightarrow O + NO \quad (R3)$$

$$N + OH \rightarrow H + NO \quad (R4)$$

Here, the first reaction is rate limiting, and because the NO levels are far below equilibrium in the flames of interest, the overall production rate may be calculated as twice the forward rate of the first reaction [15]:

$$d[NO]/dt = 2k_2[N_2][O] \quad (2)$$

where

$$k_2 = 1.84 \times 10^{11} \exp(-38{,}370/T)\ \text{mol/L s}$$

To demonstrate this approach, we consider results of measurements along a single radial profile in a non-premixed turbulent jet flame of 80% H_2 and 20% N_2 by volume. Experimental data are compared with steady strained laminar flame calculations and with a Monte Carlo PDF simulation of the turbulent flame.

Experimental Methods

The flow facility, diagnostic systems, and calibration procedures have been described previously [7,8,11]. Spontaneous Raman scattering of the beams from two Nd:YAG lasers (532 nm) was used to measure concentrations of the major species. Pulse-stretching optics were used to avoid breakdown at the focus [11], and the energies in the beams were measured by two pyroelectric joulemeters. The Rayleigh scattering signal was converted to temperature using a species-weighted scattering cross section based on the Raman measurements. Linear LIF was used to measure OH and NO, and the fluorescence signals were corrected on a shot-to-shot basis for variations in the Boltzmann fraction and the collisional quenching rate. These corrections were determined from the measured species concentrations and temperature and from published correlations for collisional quenching cross sections [16,17]. The spatial resolution for all measurements was $\sim$750 μm in each direction.

The temperature-dependent calibration functions for each of the Raman channels were determined through an extensive series of measurements in the flow above a gas heater and in flat flames above a Hencken burner [8]. Radiative losses from the calibration flames were accounted for in this procedure. Additional Raman/Rayleigh calibrations were performed immediately before and after the turbulent flame measurements. OH measurements were referenced to a H_2-air flat flame, in which the OH number density had been measured previously by laser absorption [7]. The NO calibration factor was determined by doping a lean premixed CH_4-air laminar flat flame (McKenna burner) with four known concentrations of NO. Detailed flame calculations have shown that destruction of the seeded NO in this flame is negligible [11]. The NO calibrations were also performed immediately before and after the turbulent flame measurements.

Derivation of O-atom concentrations and NO production rates depends on precision and accuracy of the measured scalars, particularly [OH] and temperature. Estimates of random errors at temperatures relevant to thermal NO production were based on the standard deviations of measured and derived scalars in steady premixed flat flames. These estimates are listed in Table 1 along with the conditions at which they were determined. Estimates of potential systematic errors are also listed in Table 1. Systematic uncertainties for [O] and d[NO]/dt were determined from Eqs. (1) and (2) as worst-case products of the contributing potential systematic errors in the measured scalars. The estimated systematic uncertainty of $\pm$80% in the NO production rate may seem high. However, we shall see that this level of quantitative information may be sufficient to distinguish between modeling approaches.

The burner was a straight tube (inner diameter, d = 4.58 mm; outer diameter, 6.34 mm; squared-off end) centered at the exit of a 30-cm by 30-cm vertical wind tunnel contraction. The co-flow air

TABLE 1
Relative standard deviations of scalars measured or derived at the listed conditions in steady flat flames and potential systematic uncertainties estimated from the calibration procedures

Scalar	σ(rms)	Conditions (mole frac., T)	Systematic Uncertainty
N_2	3%	0.71, 2140 K[a]	2%
H_2O	5%	0.18, 2140 K[a]	3%
OH	7%	0.0023, 2140 K[a]	10%
NO	10%	26, 1740 K[b]	10%
T	1%	2140 K[a]	2%
O	14%	2140 K[a]	35%
d[NO]/dt	21%	2140 K[a]	80%

[a] Premixed CH_4/air, ϕ = 0.96, uncooled burner
[b] Premixed $CH_4/O_2/N_2$, ϕ = 0.72, cooled (McKenna) burner

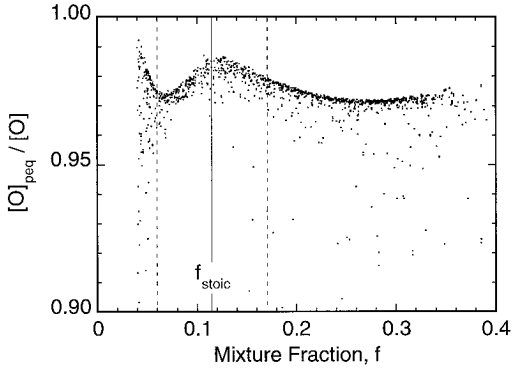

FIG. 1. Scatter plot of the ratio $[O]_{peq}/[O]$ versus mixture fraction from the PDF model simulation at $x/d = 30$, indicating the degree of departure from partial equilibrium of the reaction OH + OH = O + H_2O. The dashed lines bracket the region of interest for thermal NO formation. Data below 1200 K are not plotted.

conditions were 0.75 ± 0.05 m/s velocity, 290 K temperature, and 0.0116 H_2O mole fraction. The fuel composition was 80% H_2 and 20% N_2, by volume. The jet velocity was 151 ± 3 m/s, the exit temperature was 294 K, and the Reynolds number was 14,000, based on a mixture viscosity of $\upsilon = 4.85 \times 10^{-5}$ m^2/s. Laboratory pressure was 0.977 atm.

Measurements were made along a radial profile through the jet centerline at a streamwise distance of 30 nozzle diameters ($x/d = 30$), with 600–800 shots taken at each location. These experimental conditions were selected for several reasons. First, the spatial resolution of the system is sufficient to resolve the smallest scales at this location, as estimated following Smith et al. [18]. Second, N_2 dilution reduces the OH levels such that fluorescence trapping effects are small. Third, differential diffusion effects are not expected to be significant at this Reynolds number and streamwise location [18]. Finally, N_2 dilution reduces radiative loss, which is not included in the PDF simulation.

Monte Carlo PDF Prediction

The mean flow field was modeled by a Reynolds stress closure with a downstream marching algorithm [19]. The joint scalar PDF was solved by its modeled transport equation using the Monte Carlo technique [20]. The turbulent transport term was modeled by a gradient diffusion model using the turbulence time and fluctuating velocities from the Reynolds stress model. A modified Curl's mixing model was used to simulate the effect of turbulent stirring on the molecular diffusion process. The amount of mixing was modeled through a characteristic mixing time, which is related to the turbulence timescale. In the Monte Carlo simulation of the joint scalar PDF, the jet flame is assumed to be axisymmetric and adiabatic. Forty grid points across half of the jet were used, each containing 400 stochastic elements. The time evolution of chemical kinetics for each element was directly computed using a detailed mechanism for hydrogen combustion with NO_x chemistry that includes 14 species and 48 steps [21]. The CPU time was about 200 h on an SGI workstation for calculations up to $x/d = 150$, demonstrating that the inclusion of detailed chemistry in the PDF model is computationally expensive but not prohibitive. This simulation was based on the experimental boundary conditions of nozzle diameter, fuel composition, jet velocity, and co-flow velocity; the model was not tuned to match any aspect of the measured scalar data.

Results and Discussion

The Partial Equilibrium Assumption

Strained laminar flame calculations and perfectly stirred reactor (PSR) calculations of H_2/N_2 reacting with air were performed to assess the validity of the partial equilibrium assumption. The detailed mechanism cited previously was used, and results show that for temperatures above ~1500 K and mixtures fractions between about 0.06 and 0.17, the O-atom concentration determined from Eq. (1) differs from the actual O-atom concentration by less than 5%.

The PDF calculation can also be used to examine the partial equilibrium assumption. Figure 1 shows a scatter plot of the ratio of the partial-equilibrium O-atom concentration determined from Eq. (1) to the actual O-atom concentration predicted by the PDF simulation. For mixture fractions relevant to thermal NO formation in this flame ($0.06 < f < 0.17$), the deviation of the O-atom concentration from partial equilibrium is only 1.5–3% for the great majority of samples. We conclude that the partial equilibrium assumption is reasonable for the experimental application described here, except for determining O-atom concentrations in fuel-lean mixtures below ~1500 K.

Scatter Plots and Conditional Means

The relationships among scalars in reacting flows can be interpreted effectively when results are plotted in mixture fraction coordinates. For both experiment and prediction, the mixture fraction was calculated following the method of Bilger et al. [22] as:

$$f = \frac{(Y_H - Y_{H,2})/w_H - 2(Y_O - Y_{O,2})/w_O}{(Y_{H,1} - Y_{H,2})/w_H - 2(Y_{O,1} - Y_{O,2})/w_O}$$

where Y are elemental mass fractions, w_H and w_O

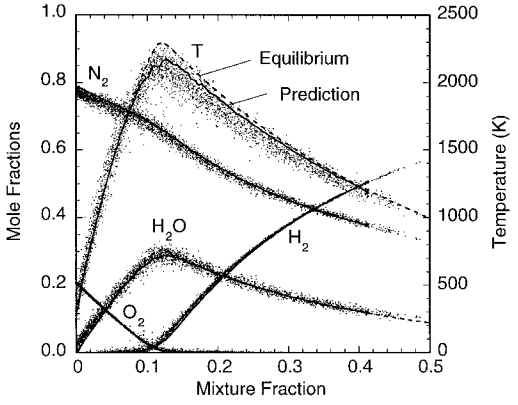

FIG. 2. Comparison of measured temperature and major species mole fractions (scatter points) with conditional averages from the PDF model prediction (———) for the streamwise location of $x/d = 30$. Equilibrium curves (- - - -) are included for temperature and H_2O.

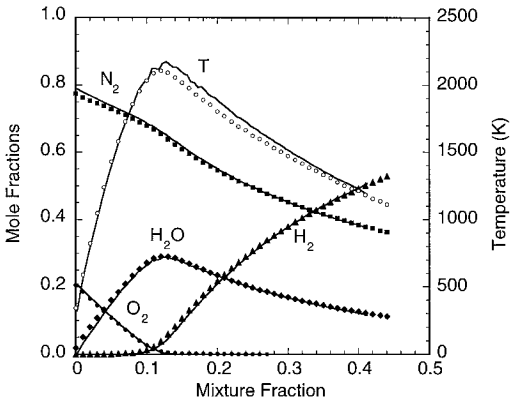

FIG. 3. Comparison of conditional averages of measured temperatures and major species mole fractions (symbols) with the corresponding predicted conditional means (———) as in Fig. 2.

are atomic weights, and the subscripts 1 and 2 refer to the fuel stream and co-flowing air stream, respectively.

Figure 2 shows scatter plots of measured temperature and the major species mole fractions. Conditional averages (conditional on mixture fraction) from the PDF calculation are shown as solid lines, and adiabatic equilibrium curves are included for H_2O and temperature. In this flame, the temperature and major species are close to equilibrium, except near the stoichiometric mixture fraction, where temperatures and H_2O mole fractions are depressed because of finite-rate chemistry. Here, results from the full radial profile are included for both experiment and prediction. In Fig. 3, conditional averages

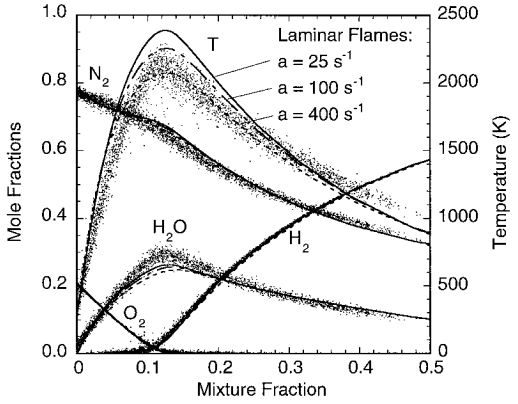

FIG. 4. Comparison of measured temperature and major species mole fractions (scatter points) with results from steady laminar flame calculations for values of the strain parameter, a, of 25 s^{-1} (———), 100 s^{-1} (— – —), and 400 s^{-1} (- - - - -).

of the measured scalars are compared with the prediction. Agreement for the major species mole fractions is very close, except for differences near $f = 0$, which arise because the calculation does not include ambient levels of H_2O and argon. The peak in the experimental temperature curve is about 50 K lower than the prediction, and the two temperature curves appear to be shifted slightly in mixture fraction relative to each other.

In Fig. 4, the experimental scatter data are compared with strained laminar flame calculations at three values of the strain parameter, a, for the Tsuji geometry. These calculations were performed using the same chemical mechanism as in the PDF simulation. They are included to illustrate that temperatures and some species mole fractions in the laminar calculations can be quite different from the turbulent flame measurements. These differences are believed to be due in part to the effects of differential diffusion being more pronounced in laminar flames [18].

Experimental and predicted results for OH mole fraction, O-atom mole fraction, NO production rate, and NO mole fraction are compared in Fig. 5. Measurements and PDF results are plotted as scatter points and conditional averages. To minimize the effect of OH fluorescence trapping, we have included only the measurements from the half of the flame profile that was closest to the fluorescence collection optics. The average fluorescence trapping effect near the center of this reaction zone was about 3%, and this correction has been applied to the OH results in this figure. Curves for the laminar flame calculations and for full adiabatic equilibrium are also included, except for NO mole fraction. NO mole fractions at equilibrium and in the laminar flames are much higher than in the turbulent flame.

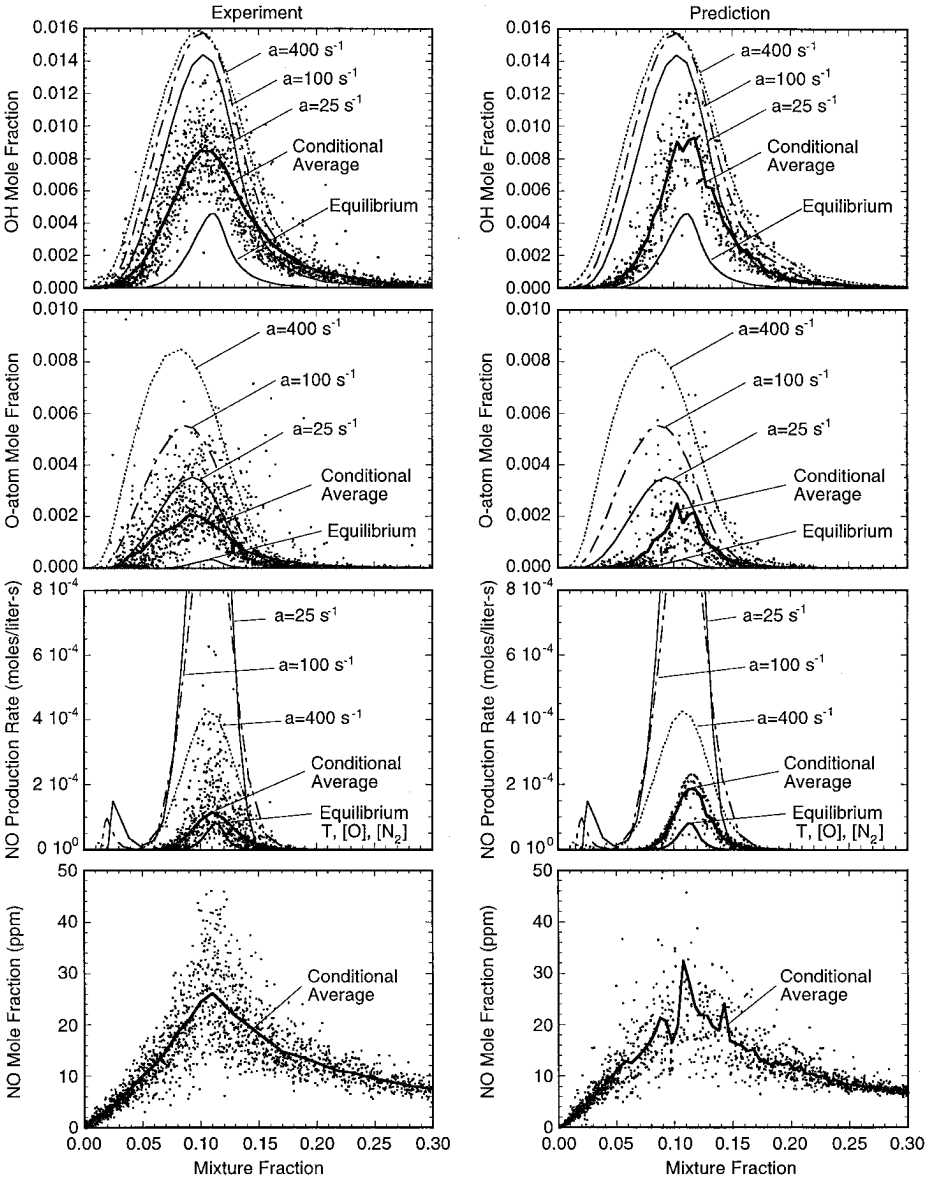

FIG. 5. Scatter plots and conditional means of experimental (left side) and predicted (right side) results for OH mole fraction, O-atom mole fraction, thermal NO production rate, and NO mole fraction at $x/d = 30$. Adiabatic equilibrium curves and results of laminar flame calculations at $a = 25\ s^{-1}$, $100\ s^{-1}$, and $400\ s^{-1}$ are included. Note that the jaggedness in the conditional averages for the prediction results from statistical noise in the Monte Carlo simulation.

There is good agreement between experiment and PDF prediction on OH mole fractions. Experimental O-atom mole fractions are significantly above equilibrium and show greater scatter than OH. The maximum in the conditionally averaged curve of experimental O-atom mole fraction is about 6.5 times that for full chemical equilibrium. The PDF prediction yields a peak value of the conditionally averaged O-atom mole fraction that is consistent with the experiment, but the experiment yields higher O-atom levels on the fuel-lean side of the peak. For mixture fractions less than about 0.06, the measured temperatures begin to drop below the range where the partial equilibrium assumption is valid and the experimental O-atom results become unreliable. This is not a problem in the context of thermal NO

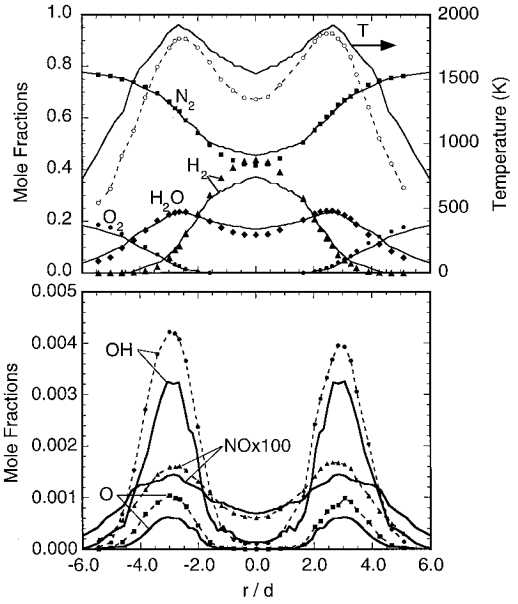

FIG. 6. Radial profiles of ensemble-average temperature and species mole fractions from the experiment (symbols) and the prediction (———) at $x/d = 30$.

production because the production rate becomes negligibly small before the partial equilibrium assumption breaks down.

The experimentally derived instantaneous NO production rates are generally greater than the curve calculated from Eq. (2) and adiabatic equilibrium values of temperature, [O], and [N_2]. The small fraction of samples that falls below this equilibrium curve may correspond to highly strained conditions in the flame, where temperature depression counters the superequilibrium O-atom levels. The widths in mixture fraction of the measured and predicted conditional average NO production curves are roughly twice that of the equilibrium curve. The experimental and predicted curves have peak values approximately 40% and 90%, respectively, above the equilibrium curve. The difference between experiment and prediction is within the estimated uncertainty in the experiment. We note that inclusion of ambient water vapor and flame radiation in the simulation is expected to decrease the predicted NO production rate, bringing it closer to the experiment.

The PDF prediction yields NO mole fractions that are close to the measurements. However, inclusion of ambient water and radiation will also reduce the predicted NO mole fraction. Firm conclusions regarding the accuracy of the PDF model in predicting NO production rates and mole fractions should not be drawn until ambient water vapor and radiation are included in the simulation, experiment and prediction may be compared at several streamwise locations, and data on the velocity field are available.

A comparison of steady laminar flame calculations with the experimental results in Fig. 5 reveals that it would not be possible to represent the turbulent flame using a combination of these laminar flames. OH levels in the laminar flames are significantly higher than both the measurements and the PDF model predictions. O-atom levels for strain rates below $a = 25\ s^{-1}$ would be consistent with the experimental results. However, the NO production rates for these weakly strained flames would greatly exceed the experimental production rates.

Radial Profiles

Radial profiles of ensemble-average temperature and species mole fractions are shown in Fig. 6. Agreement between experiment and prediction is not as good for these spatial profiles as when results are plotted against mixture fraction. The predicted temperature profile is broader than the measured profile. The predicted H_2 mole fraction on the centerline is lower than measured, and the predicted centerline temperature is higher. Within the reactions zones (near $r/d = \pm 2.5$), the predicted OH-, NO-, and O-atom mole fractions are all below the measured curves. These results show that, while the model predicts most aspects of the chemistry, it overpredicts the turbulent mixing rates such that the flame spreads too rapidly and the PDFs of mixture fraction in the reaction zones are too broad.

Conclusions

1. An experimental procedure for determining oxygen atom concentrations and instantaneous thermal NO production rates in turbulent flames was demonstrated. This procedure is based on simultaneous point measurements of temperature, the major species, and OH, and it may be applied wherever the assumption of partial equilibrium of the reaction $OH + OH \Leftrightarrow O + H_2O$ is valid.
2. Measurements were made across a radial profile at a single streamwise location, 30 nozzle diameters from the base of a turbulent jet flame of nitrogen-diluted hydrogen. The partial equilibrium assumption was shown to be valid in this flame for temperatures greater than about 1500 K. Instantaneous and conditionally averaged O-atom mole fractions at this measurement location are significantly greater than equilibrium levels. The conditional mean of the experimentally derived thermal NO production rate has a peak value 40% greater than the peak rate calculated from adiabatic equilibrium conditions of temperature, [O], and [N_2].

3. Experimental results were compared with predictions by the Monte Carlo PDF model using detailed chemistry. With some exceptions, there is good agreement between measurements and predictions when results are plotted against mixture fraction. Agreement is less good when radial profiles of ensemble-average scalars quantities are compared. This indicates that the present PDF model predicts the hydrogen and nitrogen chemistry well but that improvements are needed in the modeling of the turbulent fluid dynamics and mixing.
4. A comparison with steady strained laminar flame calculations showed that the turbulent flame measurements cannot be represented by a combination of these laminar flames.

Acknowledgments

The partial equilibrium approach was inspired in part by the insightful comments of one of the reviewers of Ref. 9. This research was supported by the U.S. Department of Energy, Office of Basic Energy Sciences. The laboratory technical support of T. Prast is gratefully acknowledged.

REFERENCES

1. Bilger, R. W. and Beck, R. E., *Fifteenth Symposium (International) on Combustion,* The Combustion Institute, Pittsburgh, 1976, pp. 541–552.
2. Drake, M. C., Correa, S. M., Pitz, R. W., Shyy, W., and Fenimore, C. P., *Combust. Flame* 69:347–365 (1987).
3. Vranos, A., Knight, B. A., Procia, W. M., and Chiapetta, L., *Twenty-Fourth Symposium (International) on Combustion,* The Combustion Institute, Pittsburgh, 1992, pp. 377–384.
4. Turns, S. R. and Lovett, J. A., *Combust. Sci. Technol.* 66:233–249 (1989).
5. Turns, S. R. and Myhr, F. H., *Combust. Flame* 87:319–335 (1991).
6. Driscoll, J. F., Chen, R.-H., and Yoon, Y., *Combust. Flame* 88:37–49 (1992).
7. Carter, C. D. and Barlow, R. S., *Opt. Lett.* 19:299–301 (1994).
8. Barlow, R. S. and Carter, C. D., *Combust. Flame* 97:261–280 (1994).
9. Barlow, R. S. and Carter, C. D., *Combust. Flame* 104:288–299 (1996).
10. Meier, W., Vyrodov, V., Bergmann, W., and Stricker, W., "Simultaneous Raman/LIF Measurements of Major Species and NO in Turbulent H_2/Air Diffusion Flames," accepted by *Appl. Phys. B.*
11. Nguyen, Q. V., Dibble, R. W., Carter, C. D., Fiechtner, G. J., and Barlow, R. S., *Combust. Flame* 105:499–510 (1996).
12. Dally, B. B., Masri, A. R., Barlow, R. S., Fiechtner, G. J., and Fletcher, D. F., *Twenty-Sixth Symposium (International) on Combustion,* The Combustion Institute, Pittsburgh, 1996, pp. 000–000.
13. Goldsmith, J. E. M., *Appl. Opt.* 26:3566–3572 (1987).
14. Smyth, K. C. and Tjossem, P. J. H., *Appl. Phys. B* 50:449–511 (1990).
15. Correa, S. M., *Combust. Sci. Technol.* 87:329–362 (1992).
16. Paul, P. H., *J. Quant. Spectrosc. Radiat. Transfer* 51:511–524 (1994).
17. Paul, P. H., Gray, J. A., Durant, J. L. Jr., and Thoman, J. W. Jr., *AIAA J.* 32:1670–1675 (1994).
18. Smith, L. L., Dibble, R. W., Talbot, L., Barlow, R. S., and Carter, C. D., *Combust. Flame* 100:153–160 (1995).
19. Chen, J.-Y., Kollmann, W., and Dibble, R. W., *Combust. Sci. Technol.* 64:315–346 (1989).
20. Pope, S. B., *Combust. Sci. Technol.* 25:159–174 (1981).
21. Gutheil, E., Balakrishnan, G., and Williams, F. A., in *Reduced Reaction Mechanisms* (Peters, N. and Rogg, B., Eds.), Springer Verlag, 1993, pp. 177–195.
22. Bilger, R. W., Starner, S. H., and Kee, R. J., *Combust. Flame* 80:135–149 (1990).

COMMENTS

A. Mokhov, N. V. Nederlandse Grasunie, The Netherlands. Did you observe partial equilibrium between the measured concentrations of OH, H_2O and O_2 on lean side and between OH, H_2O and H_2 on rich side?

Author's Reply. We have not looked for this in our data. However, based upon several papers in the literature, including work by Graham Dixon-Lewis, Jim Miller, and others, one might expect partial equilibrium of these species to be satisfied in hydrogen flames for temperatures above about 1500 K. In the present paper we have been able to extract useful information on O-atom concentrations because OH and H_2O, the measured species in the reaction $OH + OH = H_2O + O$, can be measured with useful accuracy on a single-shot basis. Our present laser systems cannot provide comparable single-shot accuracy for the Raman measurements of O_2 or H_2 because their concentrations are low in the interesting parts of the flames. In general, any evaluation of partial equilibrium in these experimental data or use of the partial equilibrium assumption in deriving new results from these data should be preceded by careful consideration of uncertainties. Unfortunately, the limitations of the O_2 and H_2 measurements also restrict our ability to derive any useful single-shot information on H-atom concentrations in these flames.